

# Scaling Behavior of InAlN/GaN HEMTs on Silicon for RF Applications

Peng Cui (✉ [pcui@sdu.edu.cn](mailto:pcui@sdu.edu.cn))

Shandong University

Yuping Zeng

University of Delaware

---

## Research Article

**Keywords:** InAlN/GaN HEMT, Si substrate,  $f_T/f_{max}$ , scale behavior.

**Posted Date:** January 3rd, 2022

**DOI:** <https://doi.org/10.21203/rs.3.rs-1216292/v1>

**License:**   This work is licensed under a Creative Commons Attribution 4.0 International License.

[Read Full License](#)

---

# Scaling behavior of InAlN/GaN HEMTs on silicon for RF applications

Peng Cui<sup>1,\*</sup> and Yuping Zeng<sup>2,\*</sup>

**Abstract**—Due to the low cost and the scaling capability of Si substrate, InAlN/GaN high-electron-mobility transistors (HEMTs) on silicon substrate have attracted more and more attentions. In this paper, a high-performance 50-nm-gate-length InAlN/GaN HEMT on Si with a high on/off current ( $I_{on}/I_{off}$ ) ratio of  $7.28 \times 10^6$ , an average subthreshold swing (SS) of 72 mV/dec, a low drain-induced barrier lowering (DIBL) of 88 mV, an off-state three-terminal breakdown voltage ( $BV_{ds}$ ) of 36 V, a current/power gain cutoff frequency ( $f_T/f_{max}$ ) of 140/215 GHz, and a Johnson's figure-of-merit (JFOM) of 5.04 THz·V is simultaneously demonstrated. The device extrinsic and intrinsic parameters are extracted using equivalent circuit model, which is verified by the good agreement between simulated and measured S-parameter values. Then the scaling behavior of InAlN/GaN HEMTs on Si is predicted using the extracted extrinsic and intrinsic parameters of devices with different gate lengths ( $L_g$ ). It presents that a  $f_T/f_{max}$  of 230/327 GHz can be achieved when  $L_g$  scales down to 20 nm with the technology developed in the study, and an improved  $f_T/f_{max}$  of 320/535 GHz can be achieved on a 20-nm-gate-length InAlN/GaN HEMT with regrown ohmic contact technology and 30% decreased parasitic capacitance. This study confirms the feasibility of further improvement of InAlN/GaN HEMTs on Si for RF applications.

**Index Terms**—InAlN/GaN HEMT, Si substrate,  $f_T/f_{max}$ , scale behavior.

## Background

InAlN/GaN high-electron-mobility transistors (HEMTs) on silicon substrate have attracted more and more attentions due to the low cost and the scaling capability of Si substrate [1-4]. L. Li *et al.* demonstrated a InAlN/GaN HEMT on Si with a gate length ( $L_g$ ) of 55 nm and a source-drain spacing ( $L_{sd}$ ) of 175 nm [5] using  $n^{++}$ -GaN regrowth source/drain contacts. The device presents a maximum drain current ( $I_{d,max}$ ) of 2.8 A/mm, a peak extrinsic transconductance ( $g_m$ ) of 0.66 S/mm, and a current/power gain cutoff frequency ( $f_T/f_{max}$ ) of 250/204 GHz. H. Xie *et al.* reported that a record  $f_T$  of 310 GHz was achieved on a InAlN/GaN HEMT on Si with a 40-nm gate length [6]. P. Cui *et al.* demonstrated an 80-nm-gate-length InAlN/GaN HEMT on Si with a record high on/off current ( $I_{on}/I_{off}$ ) ratio of  $1.58 \times 10^6$ , a steep subthreshold swing (SS) of 65 mV/dec, and a  $f_T$  of 200 GHz, resulting in a record high  $f_T \times L_g = 16$  GHz· $\mu$ m [7]. N. Chowdhury *et al.* demonstrated a complementary logic circuit (an inverter) on a GaN-on-Si platform with a record maximum voltage gain of 27 V/V at an input voltage of 0.59 V with  $V_{DD} = 5$  V [8]. H. Xie *et al.* reported an InAlN/GaN HEMT

on Si with a  $f_T$  of 210 GHz and a three-terminal off-state breakdown voltage ( $BV_{ds}$ ) of 46 V, leading to a record high Johnson's figure-of-merit (JFOM =  $f_T \times BV_{ds}$ ) of 8.8 THz·V [9].

However, to the best of our knowledge, the highest  $f_T/f_{max}$  of 454/444 GHz and 348/340 GHz were achieved on 20-nm-gate-length AlN/GaN HEMT [10] and 27-nm-gate-length InAlN/GaN HEMTs on SiC [11], respectively. Although excellent performances have been demonstrated, InAlN/GaN HEMTs on Si still presents much room to be improved compared with GaN HEMTs on SiC substrate. Hence, exploring the possible limiting factors of InAlN/GaN HEMTs on Si is significant to further improve the device performance. In this paper, high-performance InAlN/GaN HEMTs on Si are fabricated and demonstrated. The extrinsic and intrinsic parameters of devices with different gate lengths are extracted and the scale behavior of InAlN/GaN HEMTs on Si is predicted. It presents that a  $f_T/f_{max}$  of 230/327 GHz can be achieved when  $L_g$  scales down to 20 nm with the technology developed in the study, and an improved  $f_T/f_{max}$  of 320/535 GHz can be achieved on a 20-nm-gate-length InAlN/GaN HEMTs with regrowth ohmic contact technology and 30% decreased parasitic capacitance. This confirms the feasibility of further improvement of InAlN/GaN HEMTs on Si for RF applications.

## Experiment

**Figure 1(a)** shows the used lattice-matched  $\text{In}_{0.17}\text{Al}_{0.83}\text{N}/\text{GaN}$  heterostructure, which is grown on a Si substrate by metalorganic chemical vapor deposition (MOCVD). The epitaxial layer structure consists of a 2-nm GaN cap layer, an 8-nm  $\text{In}_{0.17}\text{Al}_{0.83}\text{N}$  barrier layer, a 1-nm AlN interlayer, a 15-nm GaN channel layer, a 4-nm  $\text{In}_{0.12}\text{Ga}_{0.88}\text{N}$  back-barrier layer, and a 2- $\mu$ m undoped GaN buffer layer. The electron sheet concentration and electron mobility measured by Hall measurements were  $2.28 \times 10^{13}$  cm<sup>-2</sup> and 1205 cm<sup>2</sup>/V·s, respectively.

**Figure 1(b)** shows the detailed device fabrication steps. The device fabrication started with mesa isolation using  $\text{Cl}_2/\text{CH}_4/\text{He}/\text{Ar}$  inductively coupled plasma etching. Then Ti/Al/Ni/Au stack was deposited and annealed at 850°C for 40s in  $\text{N}_2$  to form the alloyed ohmic contacts. The ohmic contact resistance is 0.3  $\Omega$ ·mm. An oxygen plasma treatment was then

\*Correspondence: [pcui@sdu.edu.cn](mailto:pcui@sdu.edu.cn); [yuzeng@udel.edu](mailto:yuzeng@udel.edu).

<sup>1</sup>Institute of Novel Semiconductors, Shandong University, Jinan, Shandong, 250100, China.

<sup>2</sup>Department of Electrical and Computer Engineering, University of Delaware, Newark, DE, 19716, USA

Full list of author information is available at the end of the article

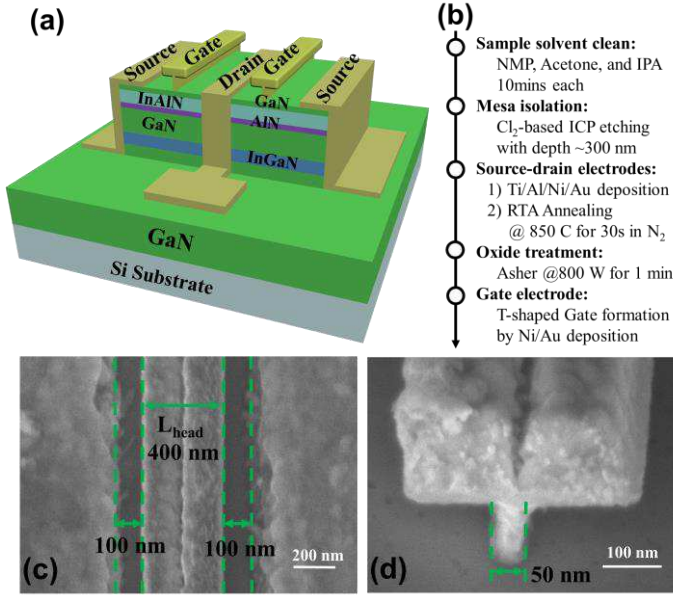


**Figure 1.** (a) Schematic of fabricated InAlN/GaN HEMT; (b) Detailed device fabrication steps; (c) a plan-view scanning electron microscopy (SEM) image of the InAlN/GaN HEMT with a gate head length ( $L_{\text{head}}$ ) of 400 nm and a source-drain spacing ( $L_{\text{sd}}$ ) of 600 nm; (d) A SEM image of T-shaped gate structure depicting a gate footprint of 50 nm.

applied to form the oxide layer on top of the InAlN layer, which can effectively reduce the gate leakage current and improve RF performance [12-15]. Finally, a Ni/Au T-shaped gate with a gate width ( $W_g$ ) of  $2 \times 20 \mu\text{m}$  was fabricated by electron beam lithography. **Figure 1(c)** shows a plan-view scanning electron microscopy (SEM) image of the InAlN/GaN HEMT with a gate head length ( $L_{\text{head}}$ ) of 400 nm and a source-drain spacing ( $L_{\text{sd}}$ ) of 600 nm. **Figure 1(d)** shows a SEM image of T-shaped gate structure depicting a gate footprint of 50 nm.

## Results and discussion

### A. DC performance

The DC current-voltage ( $I$ - $V$ ) measurements are carried out by using an Agilent B1500A semiconductor parameter analyzer. **Figure 2(a)** shows the output characteristic of the InAlN/GaN HEMT with a 50-nm gate length. The device on-resistance ( $R_{\text{on}}$ ) extracted at gate-source ( $V_{\text{gs}}$ ) of 0 V and drain-source voltage ( $V_{\text{ds}}$ ) between 0 and 0.5 V is  $1.33 \Omega\cdot\text{mm}$ . The gate-to-channel distance  $t_{\text{bar}}$  (including a 2-nm GaN, an 8-nm InAlN, and a 1-nm AlN) is 11 nm. Since  $L_g$  is 50 nm, the device presents an aspect ratio ( $L_g/t_{\text{bar}}$ ) of 4.5. Due to the low  $L_g/t_{\text{bar}}$ , the short-channel effects (SCEs) start to appear when  $V_{\text{ds}}$  is larger than 5 V and  $V_{\text{gs}}$  is between -4 to -1 V. At  $V_{\text{gs}} = 1$  V, drain current ( $I_d$ ) in saturation region presents a decrease with increased  $V_{\text{ds}}$ , an indication of the thermal effect.

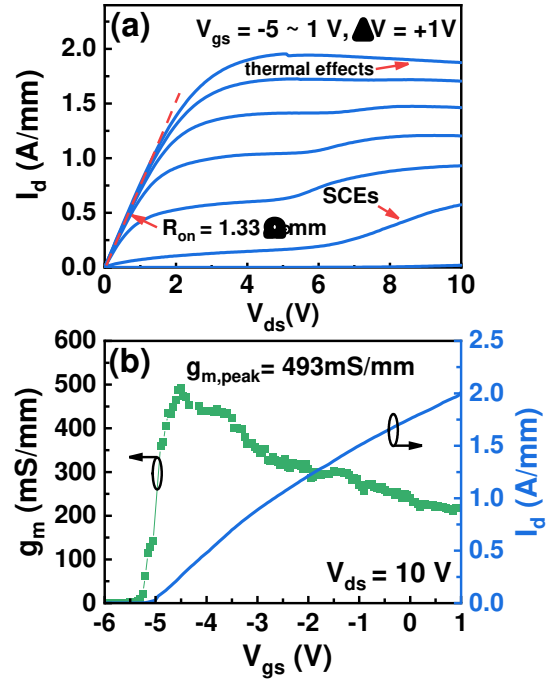


**Figure 2.** (a) Output characteristic, (b) the extrinsic transconductance  $g_m$ , and the transfer characteristic at  $V_{\text{ds}} = 10$  V of the InAlN/GaN HEMT with a 50-nm gate length.

**Figure 2(b)** shows the transfer characteristic with the extracted extrinsic transconductance ( $g_m$ ) of the InAlN/GaN HEMT with a 50-nm gate length at  $V_{\text{ds}} = 10$  V. The maximum saturation drain current ( $I_{d, \text{max}}$ ) is 2.01 A/mm at  $V_{\text{gs}} = 1$  V and  $V_{\text{ds}} = 10$  V. The  $g_m$  peak ( $g_{m, \text{peak}}$ ) is 493 mS/mm. To the best of our knowledge, the record high  $I_{d, \text{max}}$  of 2.8 A/mm and  $g_{m, \text{peak}}$  of 660 mS/mm were achieved on a 55-nm-gate-length InAlN/GaN HEMT on Si with regrowth technology and  $L_{\text{sd}}$  of 175 nm [5]. The lower both  $I_d$  and  $g_{m, \text{peak}}$  in this study result from the regrowth-free technology and the larger source-drain spacing ( $L_{\text{sd}} = 600$  nm).

**Figure 3(a)** shows the transfer and gate current ( $I_g$ ) characteristics in semi-log scale of the InAlN/GaN HEMT with a 50-nm gate length at  $V_{\text{ds}} = 5$  V and 10 V, respectively. At  $V_{\text{ds}} = 10$  V, the device off-current ( $I_{\text{off}}$ ) is  $2.76 \times 10^{-7}$  A/mm and the  $I_{\text{on}}/I_{\text{off}}$  ratio is  $7.28 \times 10^6$ , which are higher than the record reported values ( $I_{\text{off}}$  of  $7.12 \times 10^{-7}$  A/mm and  $I_{\text{on}}/I_{\text{off}}$  ratio of  $1.58 \times 10^6$ ) achieved from the InAlN/GaN HEMT on Si [16]. An average subthreshold swing (SS) of 72 mV/dec over more than two orders of  $I_d$  is extracted from the transfer curve. The drain-induced barrier lowering (DIBL) of 88 mV/V is extracted at  $I_d = 10$  mA/mm between  $V_{\text{ds}} = 10$  V and  $V_{\text{ds}} = 5$  V, which is the lowest value among the reported GaN HEMTs on Si. The lowest DIBL value suggests a suppressed SCEs for the sub-100nm gate-length device. **Figure 3(b)** shows the off-state three-terminal breakdown characteristic of the 50-nm InAlN/GaN HEMT measured at  $V_{\text{gs}} = -8$  V. The device features a  $BV_{\text{ds}}$  of 36 V at a drain leakage current of 1 mA/mm.

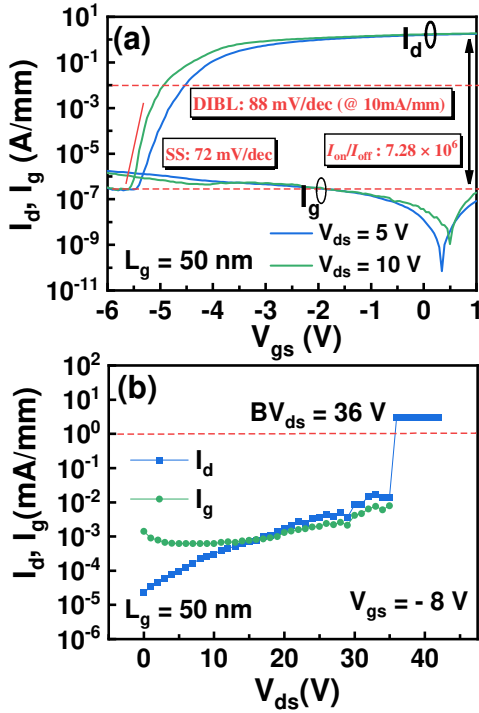


**Figure 3.** (a) The transfer and gate current characteristics in semi-log scale at  $V_{ds} = 10$  V and 5 V, (b) the  $I_d$  and  $I_g$  as a function of  $V_{ds}$  at  $V_{gs} = -8$  V of the InAlN/GaN HEMT with a 50-nm gate length. The  $BV_{ds}$  of 36 V was determined.

### B. RF performance

The device RF performance is measured with a frequency range from 1 to 65 GHz. The network analyzer is calibrated using a two-port short/open/load/through method. On-wafer open and short structures is used to eliminate the effects of parasitic elements. **Figure 4(a)** shows the the current gain ( $|h_{21}|^2$ ), unilateral gain (U), and the maximum stable gain (MSG) as a function of frequency at  $V_{ds} = 10$  V,  $V_{gs} = -3$  V after de-embedding.  $f_T/f_{max}$  of 140/215 GHz for the InAlN/GaN HEMT with a 50-nm gate length is obtained by extrapolation of  $|h_{21}|^2$  with a -20 dB/dec slope. An  $(f_T \times f_{max})^{1/2}$  of 173 GHz is obtained, which is the highest record values among the reported InAlN/GaN HEMTs on Si with regrowth-free ohmic contact technology. To the best of our knowledge, the highest  $(f_T \times f_{max})^{1/2}$  of 226 GHz ( $f_T/f_{max} = 250/204$  GHz) was achieved on a 55-nm InAlN/GaN HEMT on Si with regrowth technology. Here for our device, the alloyed ohmic resistance ( $R_C$ : 0.3  $\Omega$ ·mm) is higher than the reported regrowth ohmic contact resistance ( $R_C$ : 0.05  $\Omega$ ·mm) [5]. This presents a high potential for the RF performance improvement by further decreasing the ohmic contact resistance. Due to  $f_T/f_{max}$  of 140/215 GHz, products of  $f_T \times L_g$  and  $f_{max} \times L_g$  of 7.0 and 10.75 GHz· $\mu$ m are achieved, respectively. Although neither passivation nor field plate technology is used, the 140-GHz InAlN/GaN HEMT with an  $BV_{ds}$  of 36 V presents a Johnson's figure-of-merit (JFOM =  $f_T \times BV_{ds}$ ) of 5.04 THz·V. **Figure 4(b)** shows the measured  $f_T$  and  $f_{max}$  of the 50-nm InAlN/GaN HEMT as a function of  $V_{gs}$ . Both  $f_T$  and  $f_{max}$  show a gradual decrease compared with their peak values, presenting a good device linearity.

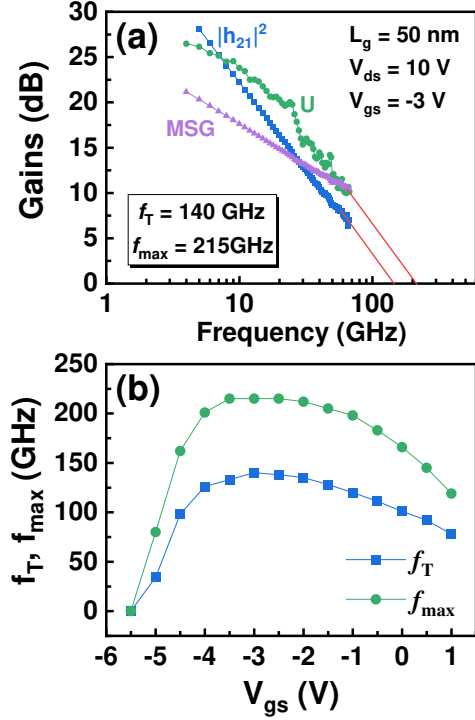


**Figure 4.** (a) RF performance of the InAlN/GaN HEMT with a 50-nm gate length at  $V_{gs} = -3$  V and  $V_{ds} = 10$  V with  $f_T/f_{max} = 140/215$  GHz. (b) The  $f_T$  and  $f_{max}$  as a function of  $V_{gs}$ .

### C. Equivalent circuit model

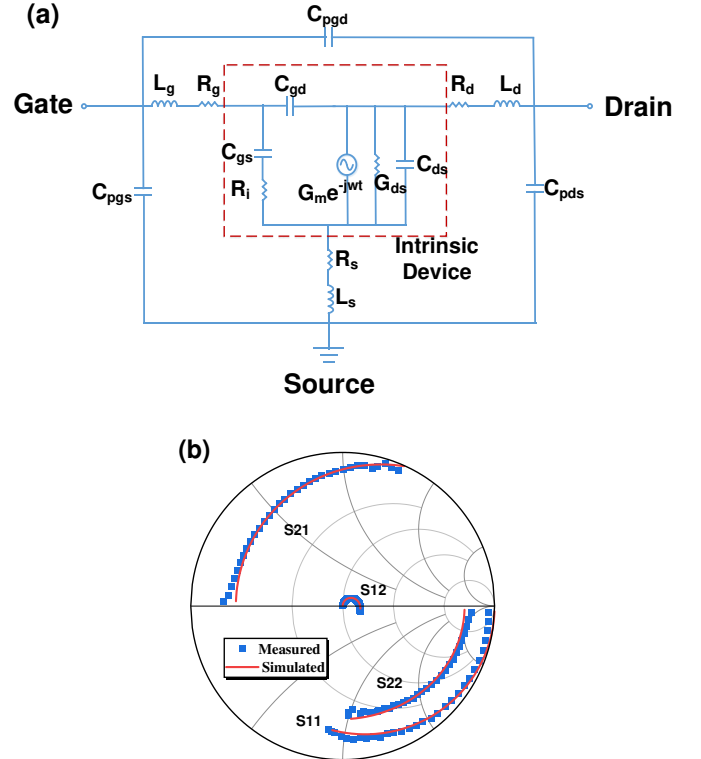


**Figure 5.** (a) Equivalent-circuit model for InAlN/GaN HEMT. The intrinsic elements are shown in the red dashed box. (b) Comparison of the simulated and measured S-parameters for the InAlN/GaN HEMT with a 50-nm gate length at  $V_{ds} = 10$  V and  $V_{gs} = -3$  V.

Table I  
THE EXTRACTED EXTRINSIC AND INTRINSIC PARAMETERS FOR THE 50-NM  
INAlN/GaN HEMTS

Extrinsic parameters	Intrinsic parameters
$C_{pgd} = 1.16$ fF	$C_{gs} = 444$ fF/mm
$C_{pgs} = 26.35$ fF	$C_{gd} = 104$ fF/mm
$C_{pds} = 26.21$ fF	$C_{ds} = 318$ fF/mm
$L_s = 3.17$ pH	$R_i = 0.90$ $\Omega \cdot \text{mm}$
$L_g = 44.03$ pH	$G_m = 573$ mS/mm
$L_d = 41.30$ pH	$G_0 = 54$ mS/mm
$R_s = 0.43$ $\Omega \cdot \text{mm}$	$G_m/G_0 = 10.6$
$R_g = 0.26$ $\Omega \cdot \text{mm}$	$\tau = 1.09$ ps
$R_d = 0.45$ $\Omega \cdot \text{mm}$	$f_{T, \text{model}} = 145$ GHz
	$f_{\text{max, model}} = 218$ GHz

The classical 16-element equivalent-circuit model is used for the InAlN/GaN HEMT, as shown in **Figure 5 (a)** [17, 18]. Based on this model, the device extrinsic and intrinsic parameters are extracted in Table I [17-19]. The slight discrepancy between the simulated and measured  $S$ -parameter values is observed in **Figure 5 (b)**, verifying the accuracy of the extracted extrinsic and intrinsic parameters. The  $f_T$  and  $f_{\text{max}}$  can be calculated using [17, 20]

$$f_T = \frac{G_m / G_0}{2\pi((C_{gs} + C_{gd})(1/G_0 + (R_s + R_d)) + (C_{gd} \cdot G_m / g_0)(R_s + R_d))}, \quad (1)$$

$$f_{\text{max}} = \frac{f_T}{2\sqrt{(R_s + R_g + R_i) \cdot G_0 + 2\pi f_T R_g C_{gd}}}.$$

where  $G_m$  and  $G_0$  are the intrinsic transconductance and drain-source conductance, respectively;  $C_{gs}$  and  $C_{gd}$  are the gate-source and gate-drain parasitic capacitance, respectively;  $R_s$ ,  $R_d$ ,  $R_g$ , and  $R_i$  are the parasitic source access resistance, drain access resistance, gate electrode resistance, and input resistance, respectively.

The calculated  $f_T/f_{\text{max}} = 145/218$  GHz is very close to the value ( $f_T/f_{\text{max}} = 140/215$  GHz) extracted by extrapolation of  $|h_{21}|^2$  with a -20 dB/dec slope, which confirms the excellent device RF performance. The high intrinsic transconductance/drain-source conductance ( $G_m/G_0$ ) ratio of 10.6 contributes to the high  $f_{\text{max}}$ .

#### D. Scaling behavior

The InAlN/GaN HEMTs with  $L_g$  between 50 nm and 350 nm are fabricated. **Figure 6(a)** shows the measured  $f_T/f_{\text{max}}$  of the InAlN/GaN HEMTs with different  $L_g$  at  $V_{gs} = -3$  V and  $V_{ds} = 10$  V. The devices with  $L_g$  of 50, 70, 100, 150, 250, and 350 nm present  $f_T/f_{\text{max}}$  of 140/215, 135/205, 120/170, 90/160, 60/136, 36/128 GHz, respectively.  $f_T \times L_g$  and  $f_{\text{max}} \times L_g$  are obtained in **Figure 6(b)**. A  $f_T \times L_g$  peak of 15 GHz $\cdot\mu\text{m}$  is achieved on the 250-nm-gate-length InAlN/GaN HEMT with a  $f_T$  of 135 GHz.  $f_{\text{max}} \times L_g$  presents a decrease from 44.8 GHz $\cdot\mu\text{m}$  ( $L_g = 350$  nm) to 10.75 GHz $\cdot\mu\text{m}$  ( $L_g = 50$  nm). The decrease of both  $f_T \times L_g$  and  $f_{\text{max}} \times L_g$  as  $L_g$  scales down means that the effect of parasitic

parameters is more pronounced, thus hindering the improvement of  $f_T$  and  $f_{\text{max}}$ . Due to the large head length of T-shaped gate ( $L_{\text{head}} = 400$  nm), the transistors features higher  $f_{\text{max}}$  and  $f_{\text{max}} \times L_g$ .

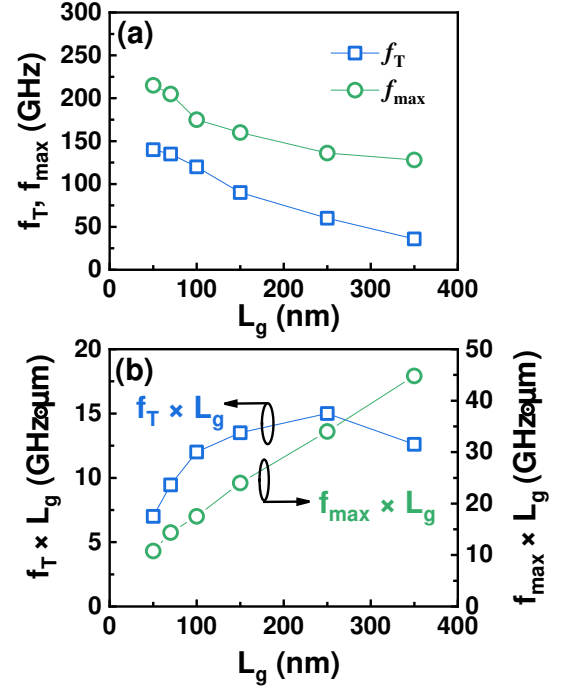


**Figure 6.** (a) Measured  $f_T$  and  $f_{\text{max}}$  as a function of  $L_g$  at  $V_{gs} = -3$  V and  $V_{ds} = 10$  V. (b)  $f_T \times L_g$  and  $f_{\text{max}} \times L_g$  as a function of  $L_g$ .

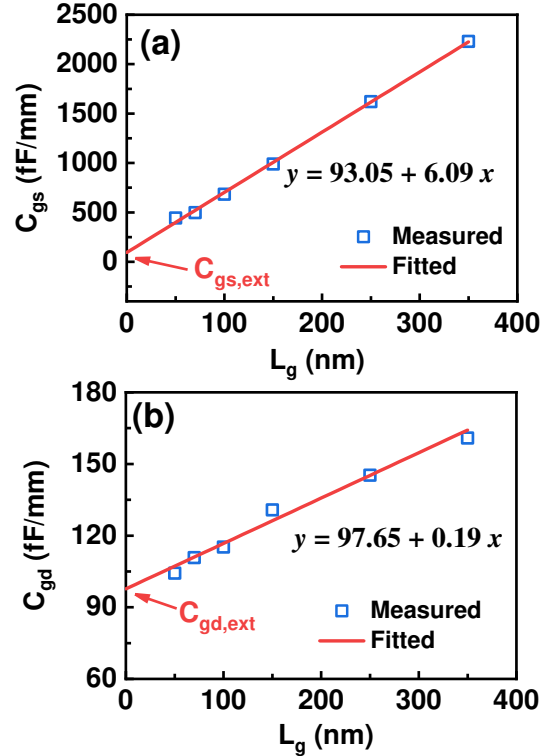


**Figure 7.** Measured and linear fitted (a) gate-source parasitic capacitance  $C_{gs}$  and (b) gate-drain parasitic capacitance  $C_{gd}$  as a function of  $L_g$  at  $V_{gs} = -3$  V and  $V_{ds} = 10$  V.

To shed more light on the scaling behavior, the extrinsic and intrinsic parameters of these devices are further extracted using the equivalent circuit model discussed above.  $C_{gs}$  can be separated to two parts: gate-source intrinsic capacitance ( $C_{gs,int}$ ) and gate-source extrinsic capacitance ( $C_{gs,ext}$ ). It means  $C_{gs} = C_{gs,int} + C_{gs,ext}$  [21].  $C_{gd}$  is the same with  $C_{gs}$  and can also be written as  $C_{gd} = C_{gd,int} + C_{gd,ext}$ . **Figure 7** shows the extracted  $C_{gs}$  and  $C_{gd}$  as a function of  $L_g$ . Both  $C_{gs}$  and  $C_{gd}$  present a linear dependence upon  $L_g$ . By linear fitting, the  $C_{gs,ext}$  and  $C_{gd,ext}$  are obtained from  $C_{gs}$  and  $C_{gd}$  at  $L_g = 0$  nm [21], as shown in **Figure 7**. Here  $C_{gs,ext}$  of 93.05 fF/mm and  $C_{gd,ext}$  of 97.65 fF/mm are determined, respectively.

The total delay ( $\tau$ ) of transistors can be written as [21] [22]

$$\tau = \frac{1}{2\pi f_T} = \tau_t + \tau_{ext} + \tau_{par} \quad (2)$$

Here  $\tau$  is partitioned into three components: transit time ( $\tau_t$ ), parasitic charging delay ( $\tau_{ext}$ ), and parasitic resistance delay ( $\tau_{par}$ ).

$\tau_t$  is the transit time under the gate region. It is related to the gate length as well as the electron velocity ( $v_e$ ) under the gate region, and can be calculated by [21, 22]

$$\tau_t = \frac{C_{gsi} + C_{gdi}}{G_m} = \frac{L_g}{v_e} \quad (3)$$

$\tau_{ext}$  is parasitic charging delay through  $C_{gs,ext}$  as well as  $C_{gd,ext}$ , and can be written as [21] [22]

$$\tau_{ext} = \frac{C_{gs,ext} + C_{gd,ext}}{G_m} \quad (4)$$

$\tau_{par}$  is parasitic resistance delay mainly associated with  $R_s$  as well as  $R_d$ , and can be written as [21] [22]

$$\tau_{par} = C_{gd}(R_s + R_d) \left[ 1 + \left( 1 + \frac{C_{gs}}{C_{gd}} \right) \frac{G_0}{G_m} \right] \quad (5)$$

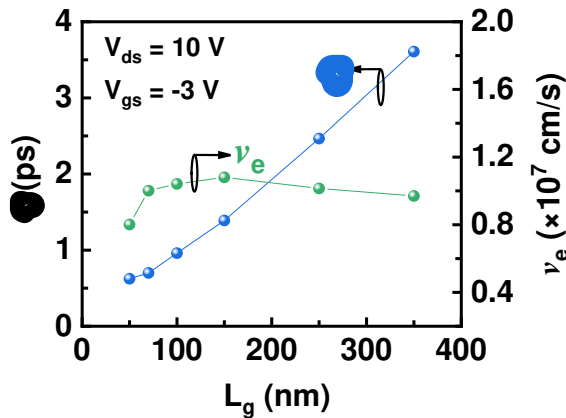


**Figure 8.** Extracted delay ( $\tau$ ) and electron velocity ( $v_e$ ) as a function of  $L_g$  at  $V_{gs} = -3$  V and  $V_{ds} = 10$  V.

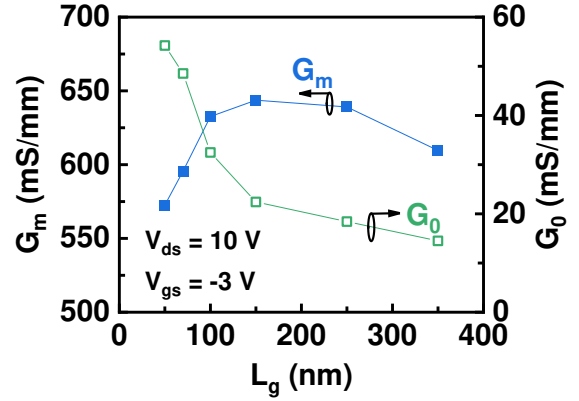


**Figure 9.** Extracted intrinsic transconductance ( $G_m$ ) and intrinsic conductance ( $G_0$ ) as a function of  $L_g$  at  $V_{gs} = -3$  V and  $V_{ds} = 10$  V.

**Figure 8** plots  $\tau$  and  $v_e$  as a function of  $L_g$  calculated from (2) and (3). As  $L_g$  decreases,  $\tau$  shows a monotonous drop, which corresponds to the increased  $f_T$ . With decreased  $L_g$ ,  $v_e$  increases to a maximum value of  $1.08 \times 10^7$  cm/s (at  $L_g = 150$  nm) and then drop to  $0.80 \times 10^7$  cm/s (at  $L_g = 50$  nm). **Figure 9** shows the extracted  $G_m$  and  $G_0$  as a function of  $L_g$ .  $G_0$  shows an increase with decreased  $L_g$ . The dependence of  $G_m$  and  $v_e$  on  $L_g$  present the same trend. Based on (3), because  $C_{gsi}$  and  $C_{gdi}$  linearly depends on  $L_g$ , we conclude that the change of  $G_m$  is attributed to  $v_e$  difference. The same trend of  $G_m$  and  $v_e$  on  $L_g$  is also observed in InAs HEMTs [23, 24] and the reason is not clear. Here we attribute it to the effect of increased electric field on the electron velocity and suggests further work is needed.

**Figure 10** exhibits the calculated  $\tau_t$ ,  $\tau_{ext}$ , and  $\tau_{par}$  using (3) to (5).  $\tau_{ext}$  and  $\tau_{par}$  is almost unchanged. Conversely,  $\tau_t$  decreases with decreased  $L_g$  and dominates the total delay in all devices. This makes it possible to decrease delay and improve  $f_T$  through downscaling of device gate length. However, for the device with  $L_g$  below 100 nm, the effect of  $\tau_{ext}$  and  $\tau_{par}$  become non-negligible. The ratios of  $(\tau_{ext} + \tau_{par})/\tau_t$  are 39% and 40% for the InAlN/GaN HEMTs with  $L_g$  of 70 and 50 nm, respectively. This means the parasitic capacitance and resistance significantly hampers further  $L_g$  scaling benefits in RF performance of sub-100 nm InAlN/GaN HEMTs.

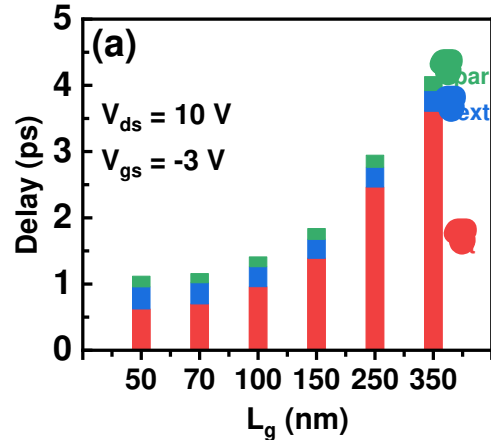


**Figure 10.** Extracted delay components as a function of  $L_g$ . The delay ( $\tau$ ) is partitioned into three components: transit time ( $\tau_t$ ), parasitic charging delay ( $\tau_{ext}$ ), and parasitic resistance delay ( $\tau_{par}$ ).

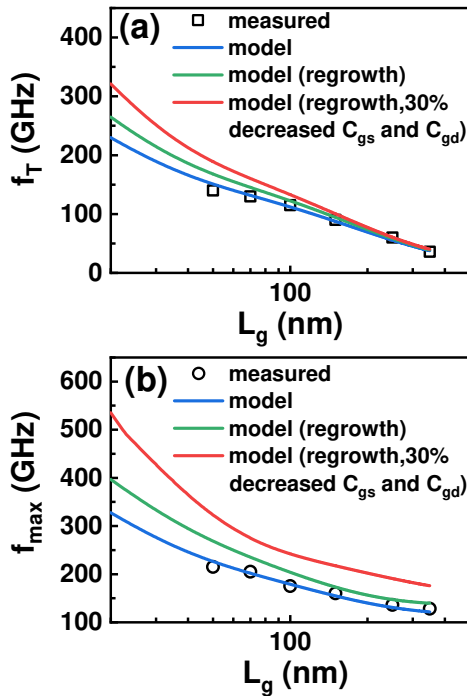


**Figure 11.**  $f_T$  and  $f_{max}$  under measured results (Scatters), obtained from model with extracted parameters (Blue-line), model with regrowth ohmic contact (Green-line), and model with regrowth and 30% decreased  $C_{gs}$  and  $C_{gd}$  (Red-line).

Therefore, downscaling and decreasing parasitic resistances as well as capacitances are very important for further improving device performance of InAlN/GaN HEMTs on Si. **Figure 11** plots the calculated  $f_T$  and  $f_{max}$  based on the model and the extracted parameters (Blue-line in **Figure 11**), which shows a good agreement with the measured results. The model results present that  $f_T/f_{max}$  of 230/327 GHz can be achieved when  $L_g$  scales down to 20 nm with the technology developed in the study. To decrease the parasitic resistance, the regrowth ohmic contact can be used. Here  $R_s$  (0.30  $\Omega$ ·mm),  $R_d$  (0.32  $\Omega$ ·mm), and  $G_m$  (573 mS/mm) are changed to 0.10  $\Omega$ ·mm, 0.08  $\Omega$ ·mm, and 620 mS/mm [5]. Then new model results with regrowth technology are plotted (Green-line in **Figure 11**) and a  $f_T/f_{max}$  of 265/397 GHz is achieved on the device with a 20-nm gate length. Optimizing the detailed structure of T-shaped gate can decrease  $C_{gs}$  and  $C_{gd}$ . Hence when 30% decreasing of  $C_{gs}$  and  $C_{gd}$  is added into the model, new results (Red-line in **Figure 11**) are plotted and an improved  $f_T/f_{max}$  of 320/535 GHz on 20-nm-gate-length InAlN/GaN HEMT is demonstrated. These values are comparable to the 27-nm InAlN/GaN HEMTs on SiC with  $f_T/f_{max}$  of 348/340 GHz, suggesting the possible of further improvement of InAlN/GaN HEMTs on Si.

## Conclusions

In summary, high-performance 50-nm InAlN/GaN HEMT on Si with an  $I_{on}/I_{off}$  ratio of  $7.28 \times 10^6$ , a SS of 72 mV/dec, a DIBL of 88 mV/V, a  $BV_{ds}$  of 36, a  $f_T/f_{max}$  of 140/215 GHz, and a JFOM of 5.04 THz·V are demonstrated. The extrinsic and intrinsic parameters of transistors with different  $L_g$  are extracted

and the scaling behavior of InAlN/GaN HEMTs on Si is demonstrated. Based on extracted model, a  $f_T/f_{max}$  of 320/535 GHz can be achieved on a 20-nm-gate-length InAlN/GaN HEMT with regrowth ohmic contact technology and 30% decreased parasitic capacitance. This study confirms the feasibility of further improvement of InAlN/GaN HEMTs on Si for RF applications.

## Supplementary Information

Not applicable.

## Abbreviations

HEMT: high-electron-mobility transistors;  $I_{on}/I_{off}$ : on/off current ratio; SS: subthreshold swing; DIBL: low drain-induced barrier lowering;  $BV_{ds}$ : off-state three-terminal breakdown voltage;  $f_T/f_{max}$ : current/power gain cutoff frequency; JFOM: Johnson's figure-of-merit;  $g_m$ : extrinsic transconductance; MOCVD: metalorganic chemical vapor deposition; SEM: scanning electron microscopy;  $I_d$ : drain current;  $I_g$ : gate current;  $L_g$ : gate length;  $L_{sd}$ : source-drain spacing;  $V_{gs}$ : gate-source voltage;  $V_{ds}$ : drain-source voltage;  $R_{on}$ : on-resistance; SCEs: short-channel effects;  $|h_{21}|^2$ : current gain; U: unilateral gain; MSG: maximum stable gain.

## Acknowledgements

Not applicable.

## Authors' Contributions

P. C. and Y. Z. contributed to the research design, experiment measurements, data analysis, and manuscript preparation. All authors reviewed this manuscript.

## Funding

This work was supported in part by the NASA International Space Station under Grant 80NSSC20M0142, and in part by Air Force Office of Scientific Research under Grant FA9550-19-1-0297 and Grant FA9550-21-1-0076.

## Availability of Data and Materials

The datasets supporting the conclusions of this article are included in the article.

## Authors' information

<sup>1</sup>Institute of Novel Semiconductors, Shandong University, Jinan, Shandong, 250100, China.

<sup>2</sup>Department of Electrical and Computer Engineering, University of Delaware, Newark, DE, 19716, USA

## Competing interests

The authors declare that they have no competing interests.

## References

- [1] K. J. Chen, O. Häberlen, A. Lidow, C. lin Tsai, T. Ueda, Y. Uemoto, and Y. Wu: GaN-on-Si power technology: Devices and applications. *IEEE Transactions on Electron Devices* 2017, 64: 779-795.
- [2] M. Ishida, T. Ueda, T. Tanaka, and D. Ueda: GaN on Si technologies for power switching devices. *IEEE Transactions on electron devices* 2013, 60: 3053-3059.
- [3] H.-S. Lee, K. Ryu, M. Sun, and T. Palacios: Wafer-level heterogeneous integration of GaN HEMTs and Si (100) MOSFETs. *IEEE Electron Device Letters* 2011, 33: 200-202.
- [4] A. Minko, V. Hoel, E. Morvan, B. Grimbert, A. Soltani, E. Delos, D. Ducatteau, C. Gaquiere, D. Theron, and J. De Jaeger: AlGaIn-GaN HEMTs on Si with power density performance of 1.9 W/mm at 10 GHz. *IEEE Electron Device Letters* 2004, 25: 453-455.
- [5] L. Li, K. Nomoto, M. Pan, W. Li, A. Hickman, J. Miller, K. Lee, Z. Hu, S. J. Bader, and S. M. Lee: GaN HEMTs on Si With Regrown Contacts and Cutoff/Maximum Oscillation Frequencies of 250/204 GHz. *IEEE Electron Device Letters* 2020, 41: 689-692.
- [6] H. Xie, Z. Liu, Y. Gao, K. Ranjan, K. E. Lee, and G. I. Ng: Deeply-scaled GaN-on-Si high electron mobility transistors with record cut-off frequency  $f_T$  of 310 GHz. *Applied Physics Express* 2019, 12: 126506.
- [7] P. Cui, A. Mercante, G. Lin, J. Zhang, P. Yao, D. W. Prather, and Y. Zeng: High-performance InAlN/GaN HEMTs on silicon substrate with high  $f_T \times L_g$ . *Applied Physics Express* 2019, 12: 104001.
- [8] N. Chowdhury, Q. Xie, M. Yuan, K. Cheng, H. W. Then, and T. Palacios: Regrowth-free GaN-based Complementary Logic on a Si Substrate. *IEEE Electron Device Letters* 2020
- [9] H. Xie, Z. Liu, Y. Gao, K. RANJAN, K. E. Lee, and G. I. Ng: CMOS-compatible GaN-on-Si HEMTs with cut-off frequency of 210 GHz and high Johnson's figure-of-merit of 8.8 THz. *V. Applied Physics Express* 2019
- [10] Y. Tang, K. Shinohara, D. Regan, A. Corrion, D. Brown, J. Wong, A. Schmitz, H. Fung, S. Kim, and M. Micovic: Ultrahigh-Speed GaN High-Electron-Mobility Transistors With  $f_T/f_{max}$  of 454/444 GHz. *IEEE Electron Device Letters* 2015, 36: 549-551.
- [11] M. L. Schuette, A. Ketterson, B. Song, E. Beam, T.-M. Chou, M. Pilla, H.-Q. Tserng, X. Gao, S. Guo, and P. J. Fay: Gate-recessed integrated E/D GaN HEMT technology with  $f_T/f_{max} > 300$  GHz. *IEEE Electron Device Letters* 2013, 34: 741-743.
- [12] J. W. Chung, J. C. Roberts, E. L. Piner, and T. Palacios: Effect of Gate Leakage in the Subthreshold Characteristics of AlGaIn/GaN HEMTs. *IEEE Electron Device Letters* 2008, 29: 1196-1198.
- [13] J. W. Chung, T.-W. Kim, and T. Palacios, "Advanced gate technologies for state-of-the-art  $f_T$  in AlGaIn/GaN HEMTs," in *2010 International Electron Devices Meeting*, 2010: 30.2. 1-30.2. 4.
- [14] D. S. Lee, J. W. W. Chung, H. Wang, X. Gao, S. P. Guo, P. Fay, and T. Palacios: 245-GHz InAlN/GaN HEMTs With Oxygen Plasma Treatment. *IEEE Electron Device Letters* 2011, 32: 755-757.
- [15] R. H. Wang, G. W. Li, O. Laboutin, Y. Cao, W. Johnson, G. Snider, P. Fay, D. Jena, and H. L. Xing: 210-GHz InAlN/GaN HEMTs With Dielectric-Free Passivation. *IEEE Electron Device Letters* 2011, 32: 892-894.
- [16] P. Cui, A. Mercante, G. Lin, J. Zhang, P. Yao, D. W. Prather, and Y. Zeng: High-performance InAlN/GaN HEMTs on silicon substrate with high  $f_T \times L_g$ . *Applied Physics Express* 2019
- [17] S. Bouzid-Driad, H. Maher, N. Defrance, V. Hoel, J.-C. De Jaeger, M. Renvoise, and P. Frijlink: AlGaIn/GaN HEMTs on Silicon Substrate With 206-GHz  $f_{max}$ . *IEEE Electron Device Letters* 2012, 34: 36-38.
- [18] G. Crupi, D. Xiao, D.-P. Schreurs, E. Limiti, A. Caddemi, W. De Raedt, and M. Germain: Accurate multibias equivalent-circuit extraction for GaN HEMTs. *IEEE transactions on microwave theory and techniques* 2006, 54: 3616-3622.
- [19] C. F. Campbell and S. A. Brown: An analytic method to determine GaAs FET parasitic inductances and drain resistance under active bias conditions. *IEEE transactions on microwave theory and techniques* 2001, 49: 1241-1247.
- [20] J. W. Chung, W. E. Hoke, E. M. Chumbes, and T. Palacios: AlGaIn/GaN HEMT With 300-GHz  $f_{max}$ . *IEEE Electron Device Letters* 2010, 31: 195-197.
- [21] D.-H. Kim, B. Brar, and J. A. Del Alamo, "f<sub>T</sub> = 688 GHz and f<sub>max</sub> = 800 GHz in L<sub>g</sub> = 40 nm In<sub>0.7</sub>Ga<sub>0.3</sub>As MHEMTs with g<sub>m,max</sub> > 2.7 mS/μm," in *2011 International Electron Devices Meeting*, 2011: 13.6. 1-13.6. 4.
- [22] D. S. Lee, X. Gao, S. P. Guo, D. Kopp, P. Fay, and T. Palacios: 300-GHz InAlN/GaN HEMTs With InGaIn Back Barrier. *IEEE Electron Device Letters* 2011, 32: 1525-1527.
- [23] D.-H. Kim and J. A. Del Alamo, "Logic performance of 40 nm InAs HEMTs," in *2007 IEEE International Electron Devices Meeting*, 2007: 629-632.
- [24] T.-W. Kim, D.-H. Kim, and J. A. del Alamo, "30 nm In<sub>0.7</sub>Ga<sub>0.3</sub>As Inverted-Type HEMTs with reduced gate leakage current for logic applications," in *2009 IEEE International Electron Devices Meeting (IEDM)*, 2009: 1-4.